HHS Public Access

Author manuscript

Calcif Tissue Int. Author manuscript; available in PMC 2016 December 01.

Published in final edited form as:

Calcif Tissue Int. 2015 December ; 97(6): 611–623. doi:10.1007/s00223-015-0055-9.

Identification and Characterization of a Synthetic Osteogenic Peptide

David E. Komatsu[1], **Michael Hadjiargyrou**[2], **Sardar MZ Udin**[1], **Nicholas A. Trasolini**[3], and **Srinivas Pentyala**[4]

[1]Stony Brook University, Department of Orthopaedics, HSC-T18, Room 085, Stony Brook, NY 11794-8181, USA

[2]New York Institute of Technology, Department of Life Sciences, Theobald Science Center, Room 420, Old Westbury, NY 11568-8000, USA

[3]Stony Brook University, School of Medicine, HSC-T4, Room 147, Stony Brook, NY 11794-8434, USA

[4]Stony Brook University, Department of Anesthesiology, HSC-L4, Room 85, Stony Brook, NY 11794-8480, USA

Abstract

Osteoporosis is the most common metabolic bone disorder and its management represents a tremendous public health encumbrance. While several classes of therapeutics have been approved to treat this disease, all are associated with significant adverse effects. An algorithm was developed and utilized to discover potential bioactive peptides, which led to the identification of an osteogenic peptide that mapped to the C-terminal region of the calcitonin receptor and has been named Calcitonin Receptor Fragment Peptide (CRFP). *In vitro* treatment of human MSCs with CRFP resulted in dose specific effects on both proliferation and osteoblastic differentiation. Similarly, *in vitro* treatment of rat RCJ cells led to dose and species specific effects on proliferation. A rat ovariectomy (OVX) model was used to assess the potential efficacy of CRFP

Corresponding Authors: David Komatsu, Department of Orthopaedics, HSC Level 18, Room 085, Stony Brook University Medical Center, Stony Brook, NY 11794-8181, david.komatsu@sbumed.org, Phone: 631-444-7222, Fax: 631-444-8894, Srinivas Pentyala, Department of Anesthesiology, HSC-L4, Room 85, Stony Brook University Medical Center, Stony Brook, NY 11794-8480, Srinivas.Pentyala@stonybrookmedicine.edu, Phone: 631-444-2974, Fax: 631-444-2907.

Contributor's Statement

Author 1 was responsible for the live animal study and analyses and oversaw study design, data analysis, data interpretation, and manuscript preparation. Author 2 oversaw cell culture studies and assisted with study design, data analysis, data interpretation, and manuscript preparation. Author 3 was responsible for the cell culture studies and assisted with data analysis and manuscript preparation. Author 4 assisted in analyzing the live animal study and assisted in data analysis and manuscript preparation. Author 5 was responsible for the bioinformatics analyses and assisted in study design, data analysis, data interpretation, and manuscript preparation. All authors revised the paper critically for intellectual content and approved the final version. All authors agree to be accountable for the work and to ensure that any questions relating to the accuracy and integrity of the paper are investigated and properly resolved.

Compliance with Ethical Standards

Author 5 is named on a pending patent related to the CRFP peptides. All other authors declare that they have no conflicts of interest relating to this work.

Research Involving Animals

All animal experiments were conducted in accordance with the United States' National Academy of Sciences' Guide for Care and Use of Laboratory Animals and were approved by the Stony Brook University Institutional Animal Care and Use Committee.

in treating osteoporosis. MicroCT analysis of distal femoral samples showed that OVX rats treated with CRFP were significantly protected from losses of 55% in trabecular bone volume fraction, 42% in connectivity density, and 18% in trabecular thickness in comparison to vehicle treated controls. MicroCT analyses of vertebrae revealed CRFP to significantly prevent a 25% reduction in bone volume fraction. MicroCT evaluation of femoral and vertebral cortical bone found a significant reduction of 2% in vertebral bone mineral density. In summary, our *in vitro* studies indicate that CRFP is both bioactive and osteogenic and our *in vivo* studies indicate that CRFP is skeletally bioactive. These promising data indicate that further *in vitro* and *in vivo* evaluation of CRFP as a new treatment for osteoporosis is warranted.

Keywords

osteoporosis; microCT; calcitonin; bioinformatics; ovariectomy

Introduction

Osteoporosis is a metabolic bone disorder characterized by a progressive reduction in bone mineral density that leads to an increased risk of bone fractures. Affecting an estimated 49 million people in the North America, the European Union, Australia, and Japan, osteoporosis is a major global public health burden [1]. Within the US, ∼9 million women are currently diagnosed with osteoporosis and this number is expected to surpass 10 million by 2020 [2]. While women are at a higher risk for developing osteoporosis, one fifth of US cases of osteoporosis and its less severe antecedent, osteopenia, occur in men [3]. As the prevalence of osteoporosis rises, so does the incidence of osteoporotic fractures, with a 2005 US incidence of ∼2 million anticipated to exceed 3 million by 2025 [4]. Concomitant with this increase in fracture incidence, the annual US direct medical expenditures associated with treating osteoporotic fractures are projected to rise from $17 billion in 2005 to $25.3 billion in 2025 [4].

Several classes of therapeutics have been approved by the FDA for the treatment of osteoporosis. The most widely prescribed are the bisphosphonates (e.g., alendronate, ibandronate), which act by inhibiting osteoclast mediated bone resorption. As a class, bisphosphonates have been shown to reduce the incidence of vertebral fractures by 40–70% and hip fractures by 40–50% [5]. Unfortunately, the long-term safety of bisphosphonate therapy is being challenged by a growing body of literature associating bisphosphonate treatment with increased incidence of osteonecrosis of the jaw and atypical subtrochanteric femoral fractures [2]. Other FDA approved anti-resorptive treatments include: hormone replacement therapy with estrogen or estrogen-progestin; raloxifene, a selective estrogen receptor modulator; calcitonin, a peptide hormone; and denosumab, a neutralizing antibody to receptor activator of nuclear factor-kappa B ligand [6]. While all of these treatments have shown some efficacy in preventing or treating osteoporosis, each one carries different risks for potentially serious adverse effects. Moreover, none of these treatments promote bone formation, an effect that would not only be beneficial in treating osteoporosis, but could also have tremendous clinical value in treating osteoporotic fractures.

Currently teriparatide is the only FDA approved osteoporosis treatment that works by promoting bone formation. Teriparatide is a recombinant peptide corresponding to the first 34 amino acids of human parathyroid hormone (PTH) and, like all other FDA approved osteoporosis treatments, has been shown to reduce the incidence of osteoporotic fractures [7]. Unfortunately, its clinical utility is hampered by a “black box warning” for a possible increased risk of osteosarcoma that restricts treatment to two years [8]. Despite this limitation, PTH has been widely evaluated as a possible treatment for enhancing fracture healing because it is the only approved skeletally anabolic agent. Indeed, numerous preclinical animal studies support the efficacy of PTH in enhancing healing under a variety of conditions [9]. Unfortunately, the sole prospective, randomized, double-blind clinical trial of teriparatide for the acceleration of fracture healing failed to support the primary hypothesis that 40ug/day would shorten time to union, although post-hoc analyses did show efficacy for 20ug/day [10].

While patients with osteoporosis now have a broad array of treatment options that significantly reduce their risk for osteoporotic fractures, no treatments are available to enhance the healing of those who do experience fractures. As fractures are the most costly and disabling sequelae of osteoporosis, the development of new osteoporosis treatments that could not only reduce fractures, but also enhance their healing, would be a tremendous public health benefit. Thus, an ideal treatment for osteoporosis would have to be multifunctional; an anabolic agent that promotes the restoration of lost bone, reduces the risk of fracture, and enhances healing when fractures do occur.

Numerous methods can be utilized to identify new therapeutics; ranging from the traditional screening of naturally derived small molecules, to more recently developed virtual screening approaches, to personalized therapeutics [11,12]. In an effort to identify new treatments options for osteoporosis, we utilized a hybrid approach to drug discovery. In the first phase, a pool of theoretically bioactive peptides was identified using a computational proteomics algorithm. The resulting peptide sequences were then aligned to identify those with significant homology to known proteins. In the next stage, the list of homologous proteins was manually reviewed to identify members of signaling pathways associated with skeletal development, homeostasis, disease, or repair. This process led to the identification of a 12-amino acid long peptide homologous to an intracellular region near the C-terminal of the calcitonin receptor and has therefore been named Calcitonin Receptor Fragment Peptide (CRFP). This report presents the results of an initial series of *in vitro* and *in vivo* experiments performed to characterize the skeletal effects of CRFP as well as assess its potential as a new treatment for osteoporosis.

Material and Methods

Algorithmic Peptide Identification

Peptide hormones and neuropeptides are synthesized and secreted as precursor proteins that typically contain Type 1 signal peptides as well as one or more Pre-pro segments that are proteolytically processed to yield the mature biopeptides. A schematic representation of a biopeptide precursor protein containing two Prepro segments is:

Signal Peptide*******//PrePro 1 //*******//PrePro 2 //*******COOH

The "*" represent "cryptic peptides" that are by products of post-translational processing. Further, the signal peptide is removed by a specific Type I signal peptidase as an integral part of the secretory process. The "//" symbols represent post-translational processing signals that include primary recognition motifs for specific endopeptidases and substrate recognition for additional enzymes that may introduce distinctive terminal structures at the ends of the mature biopeptides. These motifs that define the signal peptides, and multiple Prepro segments with complex post-translational processing signals, are very distinctive.

Based on this biological principle, we developed a computer algorithm that is capable of rapidly scanning large protein sequence databases to yield short lists of proteins highly enriched in precursors of known biopeptides. The algorithm was constructed in two stages. In the first stage, composite processing signals were constructed for multistep enzymatic processes in which the product of one enzymatic reaction becomes the substrate for the next. In the second stage, the processing signals that have been assembled along the timeline of a reaction sequence in stage one were compiled into an algorithm along the backbone sequence of a precursor protein using spacing and orientation parameters derived from known precursor proteins. The linear sequence representing the signal for the whole reaction train was thus a condensed sequence motif in which only the substrate recognition motif for the first enzymatic step was preexisting in the precursor protein sequence. In the end, sequences that survived the initial algorithm screen were submitted to programs such SignalP [13] for estimation of the probability of signal peptidase cleavage. The resulting peptide sequences were used to search the Protein Information Resource (PIR) database [14] which resulted in the identification of 123 matches out of 279,891 entries, of which nine represented known precursors of known peptide hormones. One of them was CRFP.

Peptides

Amidated CRFP peptides corresponding to human (hCRFP), rat (rCRFP), mouse (mCRFP), and scrambled human (Scr) isoforms were synthesized (GenScript, Piscataway, NJ) and resuspended in 50% DMSO (Fisher) at a stock concentration of 1mM. In addition, a fluorescein isothiocyanate (FITC) labeled form of hCRFP (FITC-CRFP), with FITC conjugated to the lysine residue, was similarly synthesized and prepared. These solutions were then sterile filtered and stored at −80°C in small aliquots. For the *in vitro* experiments, the culture media was spiked with the appropriate amount of stock solution to achieve the indicated final concentrations (1 to 10μM). For the *in vivo* experiments 15μM solutions of rCRFP in 50% DMSO, and 50% DMSO (0μM) were prepared and sterile filtered. The solutions were prepared fresh each week and stored at 4°C in aliquots sufficient for each day's injections.

Cell Culture Studies

Adult adipose derived human mesenchymal stem cells (hMSC, Lifeline Cell Technology, Frederick, MD) were cultured in maintenance (StemLife MSC Basal Media with LifeFactors Kit, Lifeline) or osteogenic (OsteoLife Complete Osteogenesis Medium, Lifeline) media and used at passage numbers < 10. Rat calvarial derived pre-chondrocytic RCJ3.1C5.18 cells

(RCJ)[15] were cultured in DMEM (Gibco, Life Technologies, Grand Island, NY) supplemented with 10% fetal bovine serum (Gibco), 1% penicillin/streptomycin (Gibco), and 10^{-7}M dexamethasone (Fisher, Pittsburgh PA) and used at passage numbers < 15. All cultures were maintained at 37°C in a humidified incubator supplemented with 5% CO_2. The media was changed every 3–4 days and the cells were passaged prior to confluence.

Localization studies were carried out using hMSC plated on 8-well chamber slides (Nunc, Rochester, NY). MSCs were plated at a density of 1×10^3 cells per chamber in maintenance media and incubated overnight. They were then incubated with FITC-CRFP or FITC-Ab (FITC-conjugated anti-mouse IgG antibodies [Sigma, St. Louis, MO]) at a concentration of 10μM for 2 hours. The cells were then washed 2×5 min with PBS (Gibco), fixed for 15 min in 4% paraformaldehyde (EMS, Hatfield), washed for 5 min with PBS, and mounted with aqueous DAPI containing medium (Vectashield, Vector labs, Burlingame, CA). The cells were then imaged using an inverted confocal microscope (Zeiss LSM 510 Two-Photon Laser Scanning Confocal Microscope, Carl Zeiss, Oberkochen, Germany).

For the proliferation studies, the cells were plated in 96-well tissue culture plates (Falcon, BD, Franklin Lakes, NJ) at a density of 4×10^3 cells per well. Twenty-four hours after plating, and daily thereafter, the media was replaced with fresh media (maintenance media for hMSC) containing CRFP of the specified species and concentration. At each of the indicated time-points proliferation was assessed by a colorimetric MTS assay (CellTiter, Promega, Madison, WI) in accordance with the manufactures directions. All experiments were performed in quadruplicate.

The osteoblastic differentiation of hMSC was determined using Alizarin red staining. Briefly, hMSC were plated in 24-well tissue culture plates (Falcon) at a density of 5×10^4 cells per well. At the indicated time-points, the cells were fixed for 1 hour at room temperature using 70% ethanol (Fisher) and then stained for 10 minutes with 40mM alizarin red (pH 4.2). The cells were next washed with tap water, dried at room temperature, and imaged with a digital camera. Following imaging, the stain was eluted from the cells by incubating them in a solution of 10% cetylpyridinium chloride (MP Biomedicals, Solon, OH) in 10mM sodium phosphate (Fisher) for 15 minutes at room temperature. The optical density of the eluted stain was then measured at 562nm using a spectrophotometer (BioTek EL800, Winooski, VT).

Live Animal Study

All animal experiments were conducted in accordance with the United States' National Academy of Sciences' Guide for Care and Use of Laboratory Animals and were approved by the Stony Brook University Institutional Animal Care and Use Committee.

Forty-eight female Sprague-Dawley rats (Charles River Laboratories, Wilmington, MA) were utilized in this study. They were retired breeders approximately 6 months old at the start of the study. One week prior to shipping, half of the rats underwent ovariectomy (OVX) surgery at the vendor's facilities while the rest of the animals did not undergo any surgical procedures (Intact). Upon arrival the rats were aged for an additional month to facilitate bone loss. The rats were allowed *ad libitum* access to food and water, lighting was

maintained in a reverse 12-hour light/dark cycle, temperature was kept at 22 ± 2°C, and humidity was constant at 50 ± 10% relative humidity.

Following aging, the OVX and Intact rats were randomized by body weight into two treatment groups, vehicle control (0μM CRFP) or treatment (15μM CRFP), resulting in a total of four treatment groups (N=12 per group): 1) Intact 0μM; 2) Intact 15μM; 3) OVX 0μM; and 4) OVX 15μM. The rats were then administered 1mL intraperitoneal injections of 0μM or 15μM rCRFP five days per week for five weeks. They were monitored daily and weighed weekly for the duration of the study. At the end of the study they were euthanized and their hind limbs and spines were collected for analysis.

MicroCT Analysis

Left femora and L5 vertebrae were scanned using a μCT 40 (Scanco Medical, Brüttisellen, Switzerland), as previously described [16–18]. For the femora, a mid-diaphyseal region of interest (ROI) consisting of 50 axial slices at was acquired at 36μm resolution to assess cortical bone properties and a distal metaphyseal ROI consisting of 617 slices was acquired at 18μm resolution to determine trabecular properties. The cortical ROI was analyzed in its entirety for cortical parameters at a threshold of 360 with sigma of 0.1, and support of 1. The trabecular analysis entailed selecting a 2mm-long sub-region located 0.5mm proximal to the growth plate and extracting the trabecular component using an automated segmentation algorithm [19]. Trabecular parameters were then analyzed at a threshold of 420 with sigma of 0.1, and support of 1.

The L5 vertebrae were scanned to acquire an ROI consisting of 412 axial slices centered at the midpoint of the vertebral body at18μm resolution. Cortical analyses were performed on 1mm-high sub-regions centered in the middle of the spinous processes at a threshold of 280 with sigma of 0.1, and support of 1. Trabecular analyses were performed on 2.5mm-long X 0.5mm diameter cylindrical sub-regions located in the center of the vertebral bodies at a threshold of 285 with sigma of 0.1, and support of 1.

Statistical Analyses

All data are presented as group mean ± standard error of the mean. Significant differences between groups were assessed using Median Tests for the cell culture studies and Kruskal-Wallis Tests for the animal study. For all tests, p-values less than 0.05 were considered significant. The analyses were performed using SPSS (Version 19, SAS Institute, Cary, NC).

Results

Peptide Identification

The algorithm was run against 279, 891 entries in Release 73 of the PIR protein sequence database and resulted in 123 hits for putative precursors of bioactive proteins. Subsequent sequence analyses of these hits using BLAST (NCBI) showed that nine corresponded to known precursors of pyroglutamyl peptide amide hormones and neuropeptides, validating the algorithm. One of the hits, a peptide with the sequence KRQWAQFKIQWNQRWGRR, was mapped to the intracellular C-terminal region of the human calcitonin receptor (Figure

1A). This region of the receptor has been shown to be its G-protein interaction site [20] and it is highly conserved across species (Figure 1B). Moreover, this peptide contains consensus sequences for processing and C-terminus amidation that result in the 12-amino acid long peptide, WAQFKIQWNQRW-amide (Figure 1C). We therefore had the following synthetic amidated peptides synthesized (GenScript USA Inc., Piscataway, NJ) for downstream experiments:

Human CRFP (hCRFP): pGlu-WAQFKIQWNQRW-amide

Rat CRFP (rCRFP): pGlu-WAQFKIQWSHRW-amide

Mouse CRFP (mCRFP): pGlu-WTQFKIQWSQRW-amide

Scrambled hCRFP (Scr): pGlu-WQRQKIWAFQNW-amide

CRFP localization

Confocal imaging of hMSCs incubated with FITC-Ab (used as a negative control) and FITC-CRFP was performed to identify the sub-cellular location of CRFP binding. Imaging was performed on clusters of cells as seen in the DAPI channel images (Figure 2AD). FITC imaging showed no signal using the FITC-Ab negative controls (Figure 2B). In contrast, FITC-CRFP cells showed distinct local regions of labeling (Figure 2E). Overlaying the DAPI, FITC, and brightfield images revealed that the FITC labeling was localized to the cell membrane of the cells in a discrete punctate manner (Figure 2F).

In Vitro Effects of CRFP on Stem Cell Proliferation and Osteogenic Differentiation

The native calcitonin receptor is highly expressed on osteoclasts and is actively shuttled to and from the cell surface [21]. Moreover, it has a number of cleavage sites that suggest an endogenous form of CRFP may exist and be involved in paracrine signaling.

We therefore exposed hMSC to hCRFP and assessed its effects on their proliferation and osteoblastic differentiation.

The overall effect of hCRFP on stem cell proliferation was modest enhancement at the highest concentration (Figure 3A). Specifically, treatment with the dose of 10μM increased proliferation on day 7 by ∼20% as compared to both scrambled control and lower concentrations of hCRFP.

The effects of hCRFP on osteoblastic differentiation of hMSC were similar to those seen for proliferation with increased mineralization visually apparent for all dose groups as compared to scrambled control at both time-points (Figure 3B). As expected, the effects of hCRFP on mineralization were most pronounced at day 12 where intense Alizarin staining is seen throughout the 1μM and 5μM hCRFP treated wells. In addition, early stimulatory effects of hCRFP can be seen on day 8, with all treated wells demonstrating more widespread staining than is seen the scrambled control. Elution of the bound dye allowed us to quantify these differences with 5μM and 10μM hCRFP showing an early stimulatory effect on differentiation characterized by increases of 72% and 105%, respectively, on day 8 in comparison to scrambled control (Figure 3C). On day 12 significant increases of 68% and

145% were seen for 1μM and 5μM hCRFP as compared to scrambled with significantly more dye also eluted from the 5μM hCRFP wells than those from 1μM hCRFP.

In Vitro effects of CRFP on Rat Chondrocyte Proliferation

Prior to conducting an ovariectomized rat study to assess the ability of CRFP to treat osteoporosis *in vivo*, a series of proliferation studies was performed on rat derived RCJ cells to optimize the CRFP isoform and dose. The dose response study was performed using rCRFP and demonstrated that both 5μM and 10μM doses were effective in increasing proliferation (Figure 4A). Specifically, 5μM rCRFP increased RCJ proliferation by 18% and 33% compared to 0μM and 1μM, respectively, on day 1, and by 81% and 26% compared to 0μM and 1μM, respectively, on day 3. Similarly, 10μM rCRFP increased proliferation by 38% compared to 1μM on day 1, 15% compared to 1μM on day 2, and 75% compared to 0μM on day 3. In contrast, 1μM only was effective on day 3 where a 44% increase was seen. With no differences seen between 5μM and 10μM rCRFP, 10μM rCRFP enhancing proliferation at all three time-points, and higher levels of proliferation seen for 10μM rCRFP at days 1 and 2, 10μM was selected as the best dose to conduct the species specificity experiments.

As expected, 10μM rCRFP enhanced RCJ proliferation with an increase of 26% compared to 0μM seen on day 2 (Figure 4B). In addition, 10μM mCRFP also stimulated proliferation with increases of 26% and 42% relative to 0μM seen on days 2 and 3, respectively. In contrast, 10μM hCRFP had a significant negative effect of proliferation, relative to 0μM, on day 1 and was indistinguishable from 0μM on days 2 and 3.

CRFP is Well Tolerated In Vivo

An OVX rat study was performed to determine if systemic treatment with CRFP is able to arrest or reverse losses in bone quantity and quality associated with osteoporosis. The *in vitro* results suggested that using either the mouse or rat CRFP isoform would lead to similar results. However, as it is possible that the murine isoform could induce an immunogenic response due to its two different amino acids, the rat isoform was utilized for these studies. The RCJ dose response experiment suggested that cellular exposure of 5μM to 10μM would be optimal. In order to attain that level of exposure at the bone we decided to treat the animals with a dose 50% higher than the upper range, to compensate for degradation and bioavailability, resulting in the selection of a 15μM dose for this study. All of the animals survived for the duration of the study and tolerated the treatments with no apparent distress or adverse effects. In addition, no pathology or gross differences between groups were seen at necropsy.

CRFP Mitigates OVX-Induced Deterioration of Skeletal Microstructure

Skeletal microstructure was assessed by microCT at cortical and trabecular regions from both femora and vertebra. Femora were selected as representative bones from the appendicular skeleton and were analyzed for cortical properties at the mid-diaphysis and trabecular properties at the distal metaphysis (Figure 5A). L5 vertebra were used to assess the axial skeleton with cortical analyses performed at center of the transverse process and trabecular analyses performed in the middle of the vertebral bodies (Figure 5B). No

differences between groups were visually apparent for the cortical ROI (data not shown). However, dramatic reductions in trabecular bone were seen in the OVX groups, particularly in the distal femoral ROI (Figure 6).

Quantification of this ROI confirmed these observations with OVX 0 rats demonstrating decreases of 55% in distal femoral bone volume fraction (BVF), 42% in connectivity density (ConnD), and 18% in trabecular thickness (TbTh) as compared to Intact 0 animals (Table 1). In addition, the structural model index (SMI) increased by 42% in OVX 0 rats, indicating that their trabeculae were more 'rod-like' and less structurally sound. Similarly BVF, ConnD, and TbTh in OVX 0 decreased in comparison to Intact 15, concomitant with an increase in SMI. In contrast, distal femoral trabeculae from OVX 15 rats were did not differ from Intact 0 or Intact 15 in any parameters except for TbTh where respective decreases of 18 and 20% were seen.

Analysis of the vertebral trabecular ROI revealed fewer differences between groups. Notably, in comparison to Intact 0, BVF was reduced by 25% in OVX 0 but did not differ in OVX 15 (Table 2). However, OVX 15 did show a 13% reduction in TbTh compared to Intact 0. There was also a direct treatment effect with OVX 15 showing a 16% reduction in trabecular spacing (TbSp) compared to OVX 0.

In contrast to the numerous differences seen in trabecular bone, the sole identified difference in cortical parameters was a 2% reduction in vertebral bone mineral density (BMD) in OVX 0 compared to Intact 0, with all other vertebral and femoral comparisons showing no differences between groups (Table 2).

Discussion

We developed an algorithm to identify novel bioactive peptides and used it to query a large protein database in an effort to identify new therapeutics for treating osteoporosis and osteoporosis related fractures. This lead to the discovery of a 12 AA-long, pyroglutamyl amidated peptide that we named calcitonin receptor fragment peptide (CRFP) due to its sequence homology with the c-terminal domain of the calcitonin receptor (CTR). Within the skeletal system, CTR expression was first identified on osteoclasts where its activation by calcitonin binding leads to G-protein mediated inhibition of osteoclast activity [22]. This understanding led to the development and approval of intranasal and subcutaneous formulations of salmon calcitonin for the treatment of osteoporosis and other metabolic disorders [23]. In addition to osteoclasts, chondrocytes also express CTR and, in contrast to osteoclasts, respond to calcitonin stimulation by increased activity (i.e., glycosaminoglycan synthesis) and proliferation [23]. As calcitonin signaling has differential effects on skeletal cells and because CRFP overlaps with the G-protein binding site of CTR, we hypothesized that CRFP would be skeletally bioactive. To test this hypothesis, a series of *in vitro* and *in vivo* studies was conducted to characterize the skeletal effects of CRFP and assess its potential as a new therapeutic to treat osteoporosis.

In vitro experiments using hMSCs revealed that hCRFP may interact with a membrane target molecule and had a dose dependent effect on both cell proliferation and

differentiation, with the highest levels of stimulation seen for concentrations of 5 and 10μM. A number of other synthetic peptides based on known osteogenic proteins such as BMP-2 [24], bone sialoprotein [25], Dkk-1 [26], and histone H4 [27] have also been shown to be effective in stimulating osteogenic differentiation and/or proliferation in hMSC. However, all of these peptides were derived from molecules known to play a role in osteogenesis. In contrast, the sequence of CFRP corresponds with a well-known constituent of a skeletally catabolic pathway. This suggests that either CTR exerts previously unknown anabolic effects or that the activity of CRFP is independent of CTR. In either case, the identification of this peptide has uncovered a novel osteogenic protein or pathway. Our results show that CRFP localized to discrete regions on the cell membrane and experiments are currently underway to elucidating precisely how CRFP acts at this location, in association with which other proteins, and on what range of cellular phenotypes.

In addition to further understanding the site and mechanism of CRFP activity, its species specificity also requires additional consideration. Despite there being only two AA substitutions between rCRFP and hCRFP or mCRFP, hCRFP had no discernible effects on the proliferation of rat derived RCJ cells. In contrast, both mCRFP and rCRFP had promoted the proliferation of RCJ cells to a similar degree. These observations indicate a need to maintain some degree of concordance between CRFP isoforms and experimental species in future experiments. Interestingly, the homology between both rat and human CRFP isoforms and rat and mouse CRFP isoforms is 83.3%. However, the substitutions in the mouse isoform are in two discrete locations whereas they are adjacent in the human isoform. This likely induces a conformational change in the human isoform that either prevents it from entering rat cells or inhibits its binding to target molecules thereby negating its activity. Based on these results and interpretations, we believed the *in vivo* OVX rat study warranted use of the rat CRFP isoform.

After electing to utilize the rat CRFP isoform for the *in vivo* experiments, the question of what dosage was considered. With no available *in vivo* data regarding pharmacokinetics or biodistribution this decision was made based on the *in vitro* studies. Optimum effects on proliferation and differentiation were seen for concentrations from 5–10μM. We therefore selected a dose of 15μM (50% higher than the high end) under the assumption that IP delivery would result in skeletal bioavailability 2–3 times lower than the injected dose. These decisions appeared prudent as several significant effects were seen in the *in vivo* study.

Specifically, the *in vivo* study revealed two key results: 1) Administration of rCRFP mitigates the detrimental effects of ovariectomy on the rat skeleton; and 2) Administration of rCRFP does not increase osteogenesis beyond the levels seen in normal (ovary intact) rat bone. These data suggest that in this model CRFP is acting by inhibiting bone resorption. However, analysis of serum C-terminal telopeptide (CTX) levels showed no differences between groups (data not shown). This argues that CRFP may stimulate bone formation solely in the context of ovariectomy, or that the effects of CRFP on osteoclasts are too subtle to be assessed by biomarker analyses. While the exact mechanism of CFRP action remains unknown, its observed osteoprotective effects are similar to those reported for calcitonin [28], indicating that CRFP may antagonize CTR in a similar manner. It is also possible that,

consistent with the *in vitro* data, CRFP exerts its activity through increased bone formation. This could occur via enhanced differentiation of bone marrow MSCs into active osteoblasts or by stimulation of existing osteoblasts to increase osteoid production. As these experiments were not explicitly designed to assess these possibilities, the precise mechanism by which CRFP protects the mammalian skeleton from ovariectomy-induced osteopenia remains to be determined.

As expected, the effects of ovariectomy were most apparent in the trabecular compartment, and in particular the distal femur. MicroCT analyses also revealed significant trabecular and cortical bone losses in the vertebral bodies. This is consistent with prior studies conducted in ovariectomized rats [29,30] as well as with clinical reports on the effects of menopause [31,32]. As such, it is not surprising that the distal femur and vertebral bodies are the sites at which we noted the greatest efficacy for CRFP in reducing OVX-induced bone loss.

Collectively, the results of these experiments demonstrate that CRFP promotes the proliferation and osteogenic differentiation of hMSC and is protective against ovariectomy-induced osteopenia in rats. However, several key questions remain unresolved. The first is the mechanism of action. As previously mentioned, there are many possible cell types, sub-cellular locations, and interacting proteins responsible for the effects of CRFP. Moreover, it may be that several signaling pathways are in fact affected by CRFP. The second major issue is determination of the optimal CRFP dosing regimen. Many assumptions were made in selecting the dose for the *in vivo* study and it is fortunate that the selected dose was able to demonstrate significant efficacy. However, optimal dosing may result in greater efficacy in preventing the development of osteopenia and perhaps even show anabolic activity and with it, the ability to treat osteoporotic fractures.

The need for effective treatments for osteoporosis and its related fractures remains large. Moreover, with only a single approved skeletally anabolic agent, there is even greater necessity for new classes of anabolic therapeutics. The identification and characterization of CRFP has shown it to be effective against OVX-induced osteopenia *in vivo* and potentially anabolic *in vitro*. Thus, this peptide represents a potentially new therapeutic approach to the development of novel treatments for osteoporosis and other disorders of bone quality.

Acknowledgements

The authors gratefully acknowledge the assistance of Anupam Sharma and Justin Smith in conducting the animal study, as well as John Glass for his support on the bioinformatics work. Research reported in this publication was supported by the Eunice Kennedy Shriver National Institute of Child Health and Human Development of the National Institutes of Health under Award Number RO1HD070888 (DEK). Additional support was provided by the NY State Biotechnology Commercialization Fund (SP) and the Stony Brook University Department of Anesthesiology.

References

1. Wade SW, Strader C, Fitzpatrick LA, Anthony MS, O'Malley CD. Estimating prevalence of osteoporosis: examples from industrialized countries. Archives of osteoporosis. 2014; 9:182. [PubMed: 24847682]
2. Shane E, Burr D, Ebeling PR, Abrahamsen B, Adler RA, Brown TD, Cheung AM, Cosman F, Curtis JR, Dell R, Dempster D, Einhorn TA, Genant HK, Geusens P, Klaushofer K, Koval K, Lane JM, McKiernan F, McKinney R, Ng A, Nieves J, O'Keefe R, Papapoulos S, Sen HT, van der

Meulen MC, Weinstein RS, Whyte M, American Society for B. Mineral R. Atypical subtrochanteric and diaphyseal femoral fractures: report of a task force of the American Society for Bone and Mineral Research. Journal of bone and mineral research : the official journal of the American Society for Bone and Mineral Research. 2010; 25(11):2267–2294.

3. Drake MT, Khosla S. Male osteoporosis. Endocrinology and metabolism clinics of North America. 2012; 41(3):629–641. [PubMed: 22877433]
4. Burge R, Dawson-Hughes B, Solomon DH, Wong JB, King A, Tosteson A. Incidence and economic burden of osteoporosis-related fractures in the United States, 2005–2025. Journal of bone and mineral research : the official journal of the American Society for Bone and Mineral Research. 2007; 22(3):465–475.
5. Khosla S, Bilezikian JP, Dempster DW, Lewiecki EM, Miller PD, Neer RM, Recker RR, Shane E, Shoback D, Potts JT. Benefits and risks of bisphosphonate therapy for osteoporosis. The Journal of clinical endocrinology and metabolism. 2012; 97(7):2272–2282. [PubMed: 22523337]
6. Schuiling KD, Robinia K, Nye R. Osteoporosis update. Journal of midwifery & women's health. 2011; 56(6):615–627.
7. Uihlein AV, Leder BZ. Anabolic therapies for osteoporosis. Endocrinology and metabolism clinics of North America. 2012; 41(3):507–525. [PubMed: 22877427]
8. Sibai T, Morgan EF, Einhorn TA. Anabolic agents and bone quality. Clinical orthopaedics and related research. 2011; 469(8):2215–2224. [PubMed: 21132409]
9. Takahata M, Awad HA, O'Keefe RJ, Bukata SV, Schwarz EM. Endogenous tissue engineering: PTH therapy for skeletal repair. Cell and tissue research. 2012; 347(3):545–552. [PubMed: 21626290]
10. Aspenberg P, Genant HK, Johansson T, Nino AJ, See K, Krohn K, Garcia-Hernandez PA, Recknor CP, Einhorn TA, Dalsky GP, Mitlak BH, Fierlinger A, Lakshmanan MC. Teriparatide for acceleration of fracture repair in humans: a prospective, randomized, double-blind study of 102 postmenopausal women with distal radial fractures. Journal of bone and mineral research : the official journal of the American Society for Bone and Mineral Research. 2010; 25(2):404–414.
11. Guido RV, Oliva G, Andricopulo AD. Modern drug discovery technologies: opportunities and challenges in lead discovery. Combinatorial chemistry & high throughput screening. 2011; 14(10): 830–839. [PubMed: 21843147]
12. Milward EA, Daneshi N, Johnstone DM. Emerging real-time technologies in molecular medicine and the evolution of integrated 'pharmacomics' approaches to personalized medicine and drug discovery. Pharmacology & therapeutics. 2012; 136(3):295–304. [PubMed: 22951096]
13. Nielsen H, Engelbrecht J, Brunak S, von Heijne G. Identification of prokaryotic and eukaryotic signal peptides and prediction of their cleavage sites. Protein engineering. 1997; 10(1):1–6. [PubMed: 9051728]
14. Wu CH, Yeh LS, Huang H, Arminski L, Castro-Alvear J, Chen Y, Hu Z, Kourtesis P, Ledley RS, Suzek BE, Vinayaka CR, Zhang J, Barker WC. The Protein Information Resource. Nucleic Acids Res. 2003; 31(1):345–347. [PubMed: 12520019]
15. Bellows CG, Aubin JE, Heersche JN, Antosz ME. Mineralized bone nodules formed in vitro from enzymatically released rat calvaria cell populations. Calcified tissue international. 1986; 38(3): 143–154. [PubMed: 3085892]
16. Warden SJ, Komatsu DE, Rydberg J, Bond JL, Hassett SM. Recombinant human parathyroid hormone (PTH 1-34) and low-intensity pulsed ultrasound have contrasting additive effects during fracture healing. Bone. 2009; 44(3):485–494. [PubMed: 19071238]
17. Komatsu DE, Brune KA, Liu H, Schmidt AL, Han B, Zeng QQ, Yang X, Nunes JS, Lu Y, Geiser AG, Ma YL, Wolos JA, Westmore MS, Sato M. Longitudinal in vivo analysis of the region-specific efficacy of parathyroid hormone in a rat cortical defect model. Endocrinology. 2009; 150(4):1570–1579. [PubMed: 19022894]
18. Komatsu DE, Bosch-Marce M, Semenza GL, Hadjiargyrou M. Enhanced bone regeneration associated with decreased apoptosis in mice with partial HIF-1alpha deficiency. Journal of bone and mineral research : the official journal of the American Society for Bone and Mineral Research. 2007; 22(3):366–374.

19. Lublinsky S, Ozcivici E, Judex S. An automated algorithm to detect the trabecular-cortical bone interface in micro-computed tomographic images. Calcified tissue international. 2007; 81(4):285–293. [PubMed: 17828460]

20. Orcel P, Tajima H, Murayama Y, Fujita T, Krane SM, Ogata E, Goldring SR, Nishimoto I. Multiple domains interacting with Gs in the porcine calcitonin receptor. Molecular endocrinology. 2000; 14(1):170–182. [PubMed: 10628756]

21. Seck T, Baron R, Horne WC. Binding of filamin to the C-terminal tail of the calcitonin receptor controls recycling. The Journal of biological chemistry. 2003; 278(12):10408–10416. [PubMed: 12531889]

22. Davey RA, Findlay DM. Calcitonin: physiology or fantasy? Journal of bone and mineral research : the official journal of the American Society for Bone and Mineral Research. 2013; 28(5):973–979.

23. Karsdal MA, Henriksen K, Arnold M, Christiansen C. Calcitonin: a drug of the past or for the future? Physiologic inhibition of bone resorption while sustaining osteoclast numbers improves bone quality. BioDrugs : clinical immunotherapeutics, biopharmaceuticals and gene therapy. 2008; 22(3):137–144.

24. Kang EJ, Kim SK, Eom TG, Choi KO, Lee TH. Evaluation of the osteogenic activity of the BMP-2 mimetic peptide, PEP7, in vitro and in vivo. The International journal of oral & maxillofacial implants. 2013; 28(3):749–756. [PubMed: 23748305]

25. Choi YJ, Lee JY, Lee SJ, Chung CP, Park YJ. Determination of osteogenic or adipogenic lineages in muscle-derived stem cells (MDSCs) by a collagen-binding peptide (CBP) derived from bone sialoprotein (BSP). Biochemical and biophysical research communications. 2012; 419(2):326–332. [PubMed: 22342728]

26. Gregory CA, Perry AS, Reyes E, Conley A, Gunn WG, Prockop DJ. Dkk-1-derived synthetic peptides and lithium chloride for the control and recovery of adult stem cells from bone marrow. The Journal of biological chemistry. 2005; 280(3):2309–2323. [PubMed: 15504735]

27. Bab I, Gazit D, Chorev M, Muhlrad A, Shteyer A, Greenberg Z, Namdar M, Kahn A. Histone H4-related osteogenic growth peptide (OGP): a novel circulating stimulator of osteoblastic activity. The EMBO journal. 1992; 11(5):1867–1873. [PubMed: 1582415]

28. Rico H, Valencia MJ, Villa LF, Hernandez ER, Seco C, Sanchez-Atrio A, Revilla M. Calcitonin versus clodronate in the prevention of ovariectomy-induced osteopenia in rats. Clinical rheumatology. 2000; 19(1):47–50. [PubMed: 10752499]

29. Campbell GM, Buie HR, Boyd SK. Signs of irreversible architectural changes occur early in the development of experimental osteoporosis as assessed by in vivo micro-CT. Osteoporosis international : a journal established as result of cooperation between the European Foundation for Osteoporosis and the National Osteoporosis Foundation of the USA. 2008; 19(10):1409–1419.

30. Francisco JI, Yu Y, Oliver RA, Walsh WR. Relationship between age, skeletal site, and time post-ovariectomy on bone mineral and trabecular microarchitecture in rats. Journal of orthopaedic research : official publication of the Orthopaedic Research Society. 2011; 29(2):189–196. [PubMed: 20722002]

31. Jiang Y, Zhao J, Liao EY, Dai RC, Wu XP, Genant HK. Application of micro-CT assessment of 3-D bone microstructure in preclinical and clinical studies. Journal of bone and mineral metabolism. 2005; 23(Suppl):122–131. [PubMed: 15984427]

32. Akhter MP, Lappe JM, Davies KM, Recker RR. Transmenopausal changes in the trabecular bone structure. Bone. 2007; 41(1):111–116. [PubMed: 17499038]

A

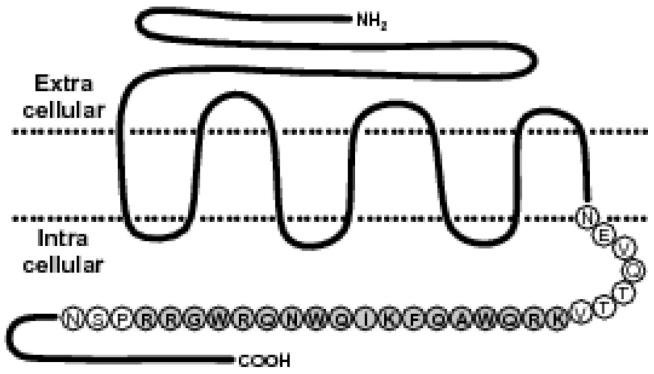

B

Species	Peptide Sequence
Human	KRQWAQFKIQWNQRWGRR
Rat	KRQWAQFKIQW**SH**RWGRR
Mouse	KRQW**T**QFKIQW**S**QRWGRR

C

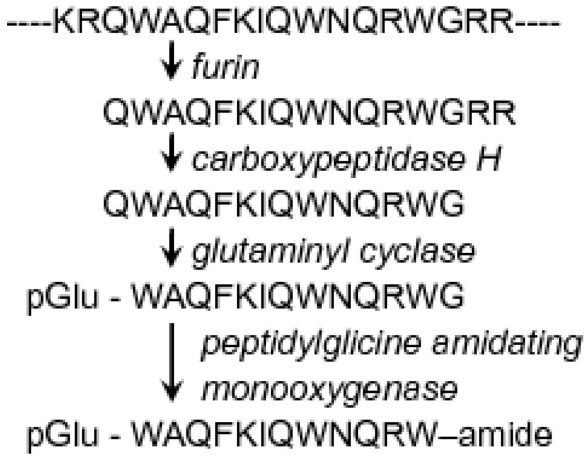

Fig 1. Calcitonin Receptor Fragment Peptide (CRFP)

A) Schematic representation of the human calcitonin receptor, a 7 pass transmembrane G-protein coupled receptor, with the 18 AA-long CRFP sequence from the intracellular C-terminal region shown in bold. **B)** Peptide sequences of the human, rat, and mouse CRFP homologues. The sequences are highly conserved and deviations from the human sequence are indicated in bold. **C)** Amidation reaction required to stabilize and induce biological activity of CRFP, enzymes (in italics) sequentially modify the indicated residues (in bold) to yield the mature 12 AA-long pyroglutimated and amidated CRFP.

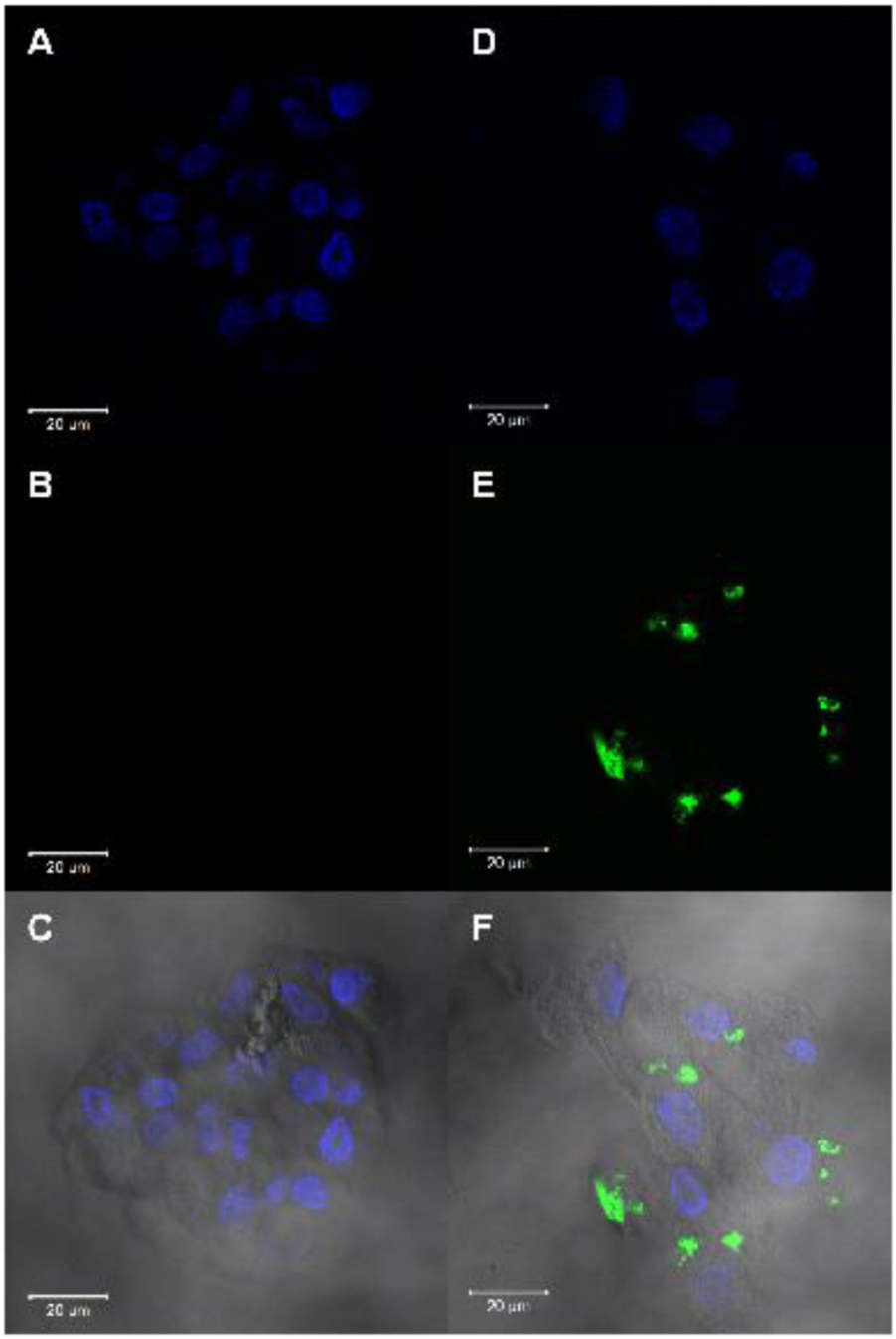

Fig 2. CRFP Localization

Confocal microscopic imaging of hMSC treated with FITC-CRFP and FITC-Ab (negative control), counterstained with DAPI to show nuclei. **A)** Epifluorescence imaging of DAPI on control slide. **B)** Epifluorescence imaging of FITC on control slide. **C)** Overlay of DAPI, FITC, and brightfield images on control slide. **D)** Epifluorescence imaging of DAPI on experimental slide. **E)** Epifluorescence imaging of FITC on experimental slide. F) Overlay of DAPI, FITC, and brightfield images of experimental slide. For all images, scale bar = 20μm.

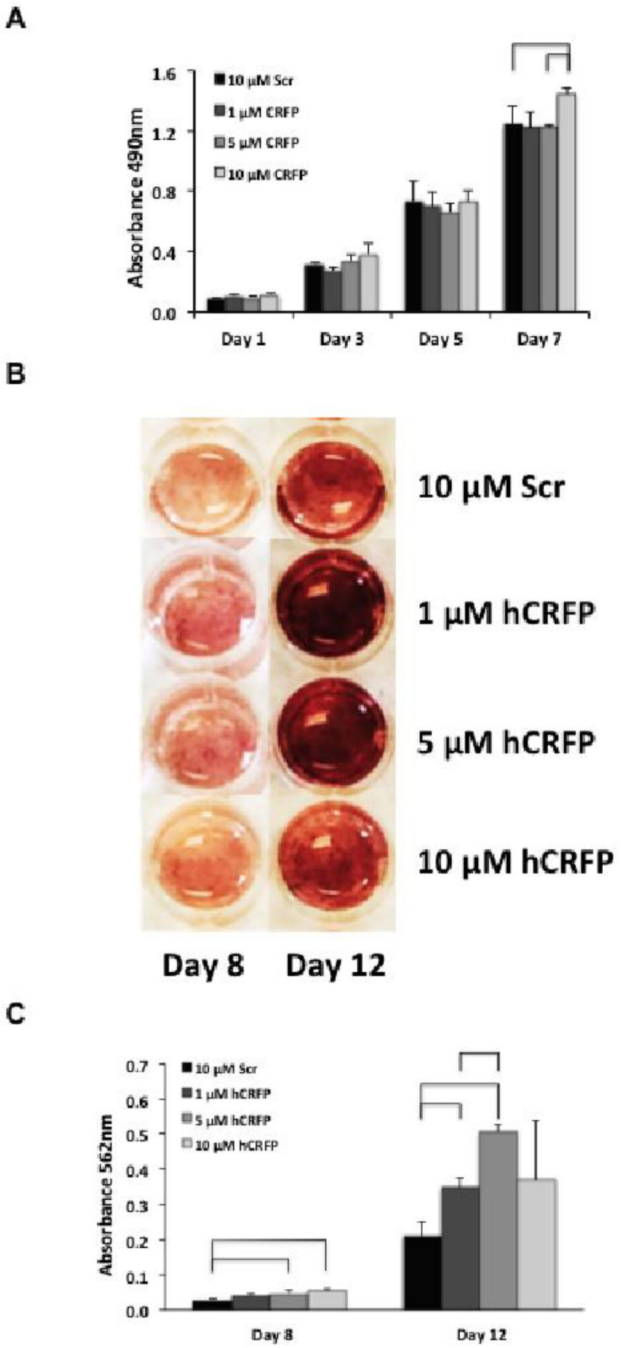

Fig 3. CRFP treatment has dose dependent effects on the proliferation and osteogenic differentiation of adult mesenchymal stem cells

A) Bar graph showing proliferation of adipose-derived hMSC in response to treatment with scrambled hCRFP and hCRFP at concentrations of 1, 5, and 10μM. Proliferation was measured on days 1, 3, 5, and 7 using an MTS assay and the results plotted as average ± SEM. Comparisons were made between groups at each time-point using Median Tests (SPSS) and considered significant for p-values < 0.05. Groups that differ are denoted with brackets. **B)** Images of hMSC stained with Alizarin to assess matrix mineralization (red), an

indicator of osteogenic differentiation, following 8 and 12 days of treatment with scrambled hCRFP and hCRFP at concentrations of 1, 5, and 10μM. **C)** Bar graph showing quantitative results of the matrix mineralization assay as determined by eluting and measuring the amount of bound Alizarin spectrophotometrically. Comparisons were made between groups at each time-point using Median Tests (SPSS) and considered significant for p-values < 0.05. Groups that differ are denoted with brackets.

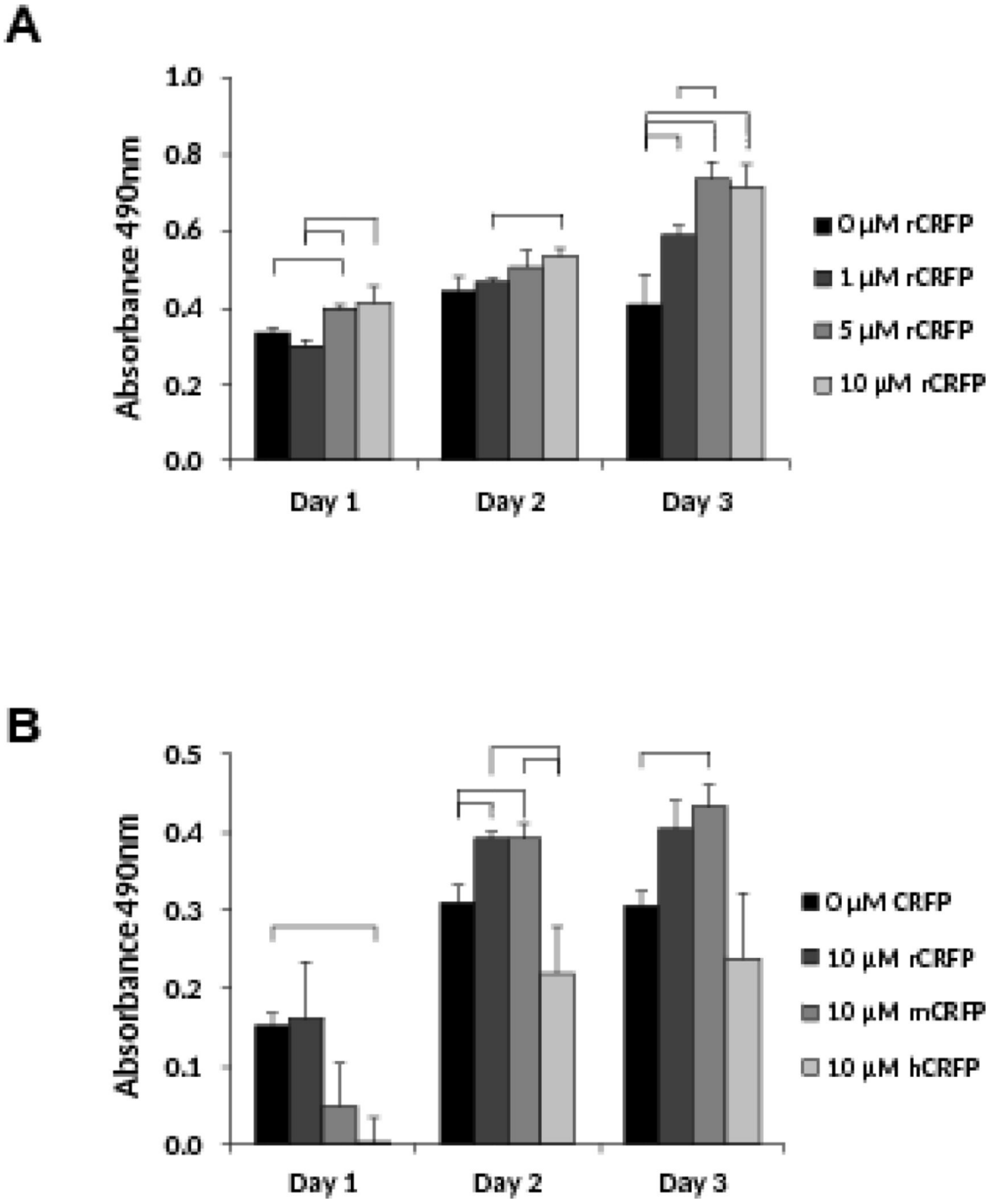

Fig 4. CRFP treatment has dose dependent and species specific effects on rat chondrocyte proliferation

A) Bar graph showing proliferation of RCJ cells in response to treatment with rCRFP at concentrations of 0, 1, 5, and 10µM. Proliferation was measured on days 1, 2, and 3, using an MTS assay and the results plotted as average ± SEM. Comparisons were made between groups at each time-point using Median Tests (SPSS) and considered significant for p-values < 0.05. Groups that differ are denoted with brackets. **B)** Bar graph showing proliferation of RCJ cells in response to treatment with 0µM CRFP, as well as 10µM rCRFP,

mCRFP, and hCRFP. Proliferation was measured on days 1, 2, and 3, using an MTS assay and the results plotted as average ± SEM. Comparisons were made between groups at each time-point using Median Tests (SPSS) and considered significant for p-values < 0.05. Groups that differ are denoted with brackets.

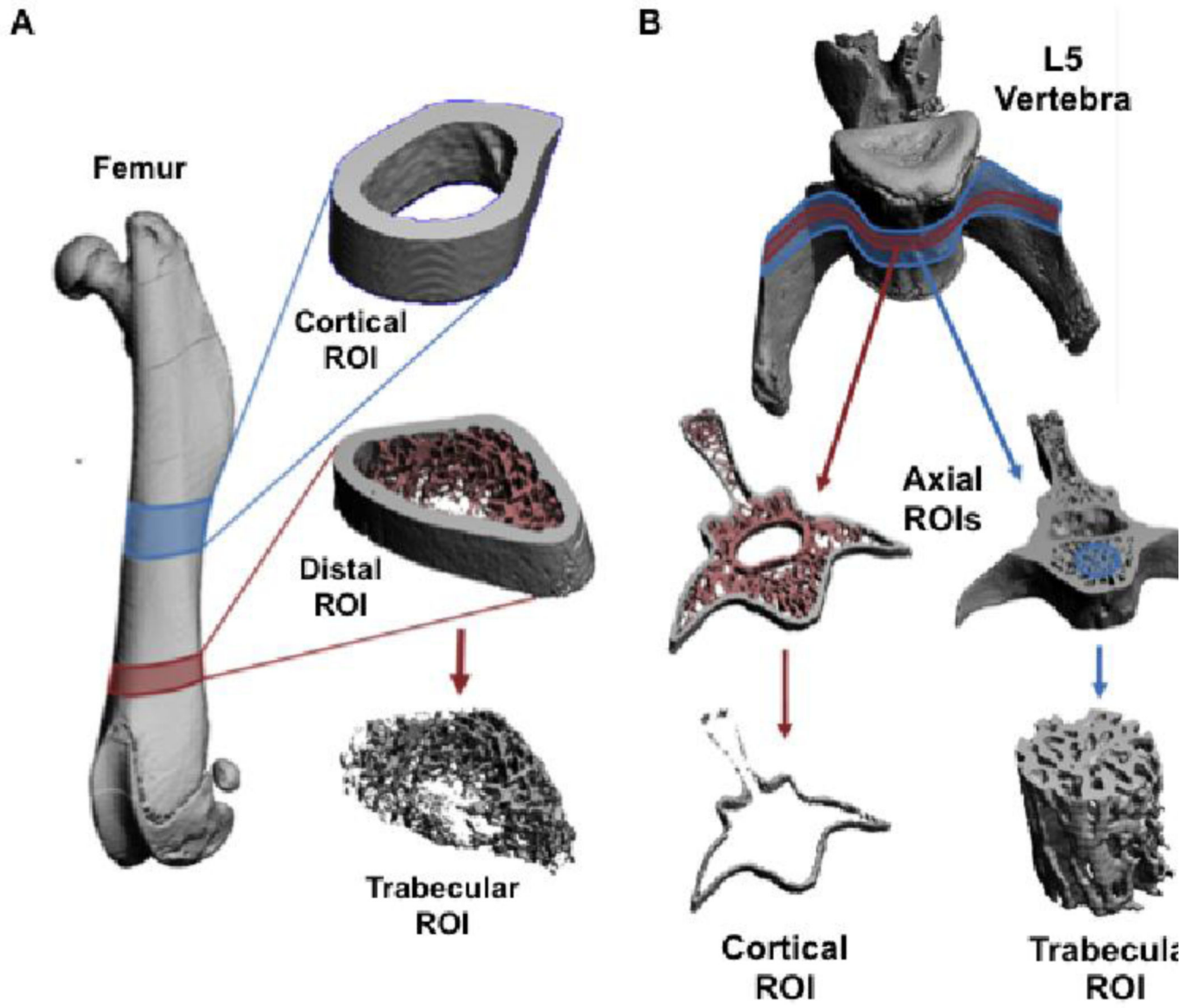

Fig 5. MicroCT Regions of Interest

A) Surface rendered images from a microCT scanned femur and magnified views of the ROIs used for quantitative analyses. The location of the midshaft cortical ROI is highlighted in blue and that of the distal trabecular ROI is highlighted in red. The distal ROI is shown as a segmented image and as the isolated trabecular ROI. **B)** Surface rendered images from a microCT scanned L5 vertebra with magnified views of the ROIs used for quantitative analyses. A thin axial ROI, highlighted in red, was segmented to remove the trabecular bone and isolate the cortical ROI. A thicker axial ROI, highlighted in blue, had a cylinder positioned through the vertebral body to isolate the trabecular ROI.

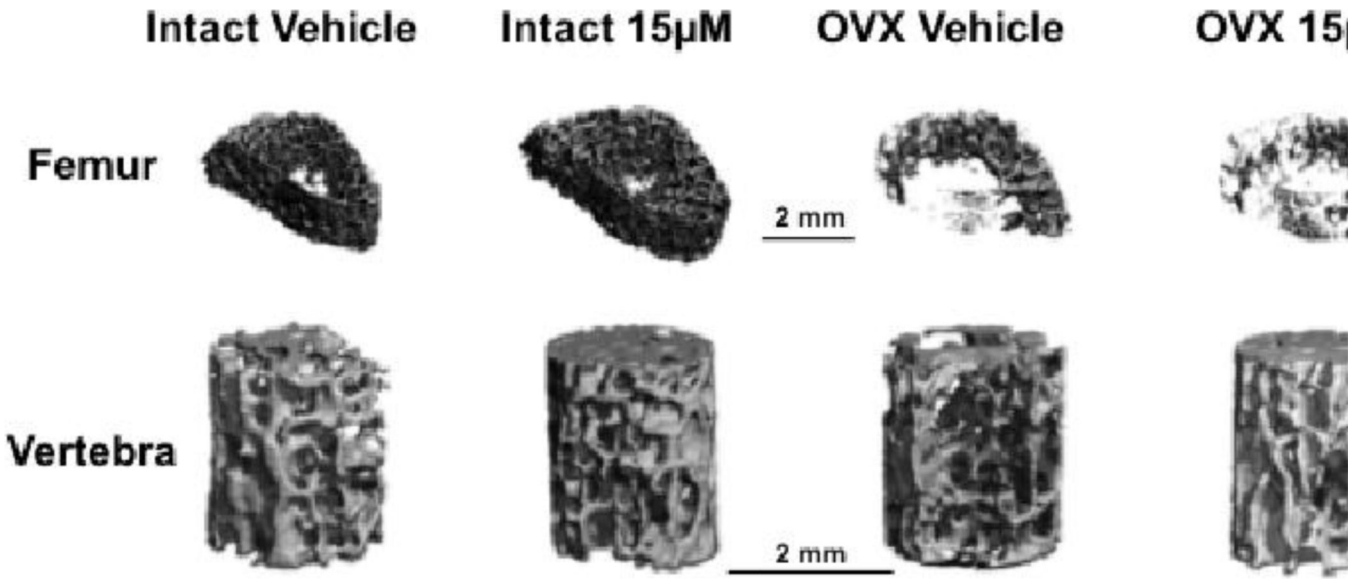

Fig 6. Trabecular MicroCT images

Representative series of surface rendered microCT images of trabecular ROI from femora and vertebra collected from Intact and OVX rats treated with 0 and 15μM rCRFP for 5 weeks. Trabeculae in the OVX rats appear thinner and sparser, particularly in the femoral images. Scale bars = 2mm.

Table 1

Femoral microCT properties

		Intact 0μM	Intact 15μM	OVX 0μM	OVX 15μM	p-value	Pairwise Comparisons
		Mean SEM	Mean SEM	Mean SEM	Mean SEM		
Distal Trabecular MicroCT	**Bone Volume Fraction**	**0.1608** ± 0.0177	**0.1534** ± 0.0231	**0.0719** ± 0.0108	0.0920 ± 0.0178	0.001	a, b
	Connectivity Density (1/mm^3)	**63.6576** ± 5.3309	**64.6827** ± 9.7038	**36.9534** ± 5.0976	49.3944 ± 6.6693	0.003	a, b
	Structural Model Index	**1.7150** ± 0.1898	**1.7297** ± 0.1469	**2.4367** ± 0.1283	2.2821 ± 0.1473	0.001	a, b
	Trabecular Number (1/mm)	2.4845 ± 0.2531	2.4311 ± 0.3253	1.6734 ± 0.1229	1.9470 ± 0.2082	0.048	-
	Trabecular Thickness (mm)	**0.0801** ± 0.0030	**0.0816** ± 0.0035	**0.0656** ± 0.0029	**0.0653** ± 0.0035	0.000	a, b, c, d
	Trabecular Spacing (mm)	0.4849 ± 0.0590	0.4961 ± 0.0484	0.6533 ± 0.0539	0.5915 ± 0.0546	0.066	-
	BMD(mgHA/cm^3)	741.7345 ± 3.8979	745.9079 ± 6.3025	740.1545 ± 5.9500	733.5584 ± 3.7173	0.494	-
Midshaft Cortical MicroCT	**Periosteal Volume (mm^3)**	20.4740 ± 0.4266	21.5651 ± 0.7082	21.2870 ± 0.4501	21.8137 ± 0.5349	0.349	-
	Bone Volume (mm^3)	12.5893 ± 0.3238	12.6553 ± 0.6145	12.4532 ± 0.3993	12.5053 ± 0.3441	0.992	-
	Endosteal Volume (mm^3)	7.9893 ± 0.3243	9.9756 ± 0.8365	8.9206 ± 0.4139	9.3785 ± 0.4628	0.080	-
	Cortical Thickness (mm)	0.7001 ± 0.0191	0.6811 ± 0.0306	0.6756 ± 0.0239	0.6683 ± 0.0239	0.764	-
	Polar Momment of Inertia (mm^4)	18.7315 ± 0.7439	20.2682 ± 1.4546	19.6494 ± 0.8299	20.3704 **i** 0.8854	0.738	-
	BMD (mg HA/cm^3)	969.4624 ± 2.9323	972.7679 ± 7.7914	976.3143 ± 7.4967	963.6538 ± 2.6947	0.347	-

This table presents results of the femoral microCT analyses. The upper rows present data obtained from the trabecular bone in the distal portion of the femora. The lower rows present data obtained from the cortical bone in the mid-diaphyseal portion of the femora. The first column lists the MicroCT parameters and the units. The next four columns present the group means ± standard error of the mean. The next column presents the p-values arising from between group comparisons performed using Kruskal-Wallis tests. The final column reveals the pairs that were found to be significantly different (a = Intact 0 vs. OVX 0; b = Intact 15 vs. OVX 0; c = Intact 15 vs. OVX 15; d = Intact 0 vs. OVX 15; e = OVX 0 vs. OVX 15). In addition, means that differ significantly have been presented in bold.

Table 2

Vertebral microCT properties

		Intact 0μM	Intact 15μM	OVX 0μM	OVX 15μM	p-value	Pairwise Comparisons
		Mean SEM	Mean SEM	Mean SEM	Mean SEM		
Distal Trabecular MicroCT	**Bone Volume Fraction**	**0.1608** ± 0.0177	**0.1534** ± 0.0231	**0.0719** 1 0.0108	0.0920 ± 0.0178	0.001	a, b
	Connectivity Density (1/mm^3)	**63.6576** ± 5.3309	**64.6827** ± 9.7038	**36.9534** 1 5.0976	49.3944 ± 6.6693	0.003	a, b
	Structural Model Index	**1.7150** ± 0.1898	**1.7297** ± 0.1469	**2.4367** 1 0.1283	2.2821 ± 0.1473	0.001	a, b
	Trabecular Number (1/mm)	2.4845 ± 0.2531	2.4311 ± 0.3253	1.6734 ± 0.1229	1.9470 ± 0.2082	0.048	-
	Trabecular Thickness (mm)	**0.0801** ± 0.0030	**0.0816** ± 0.0035	**0.0656** ± 0.0029	**0.0653** ± 0.0035	0.000	a, b, c, d
	Trabecular Spacing (mm)	0.4849 ± 0.0590	0.4961 ± 0.0484	0.6533 ± 0.0539	0.5915 ± 0.0546	0.066	-
	BMD (mg HA/cm^3)	741.7345 ± 3.8979	745.9079 ± 6.3025	740.1545 ± 5.9500	733.5584 ± 3.7173	0.494	-
Midshaft Cortical MicroCT	**Periosteal Volume (mm^3)**	20.4740 ± 0.4266	21.5651 ± 0.7082	21.2870 ± 0.4501	21.8137 ± 0.5349	0.349	-
	Bone Volume (mm^3)	12.5893 ± 0.3238	12.6553 ± 0.6145	12.4532 + 0.3993	12.5053 ± 0.3441	0.992	-
	Endosteal Volume (mm^3)	7.9893 ± 0.3243	9.9756 ± 0.8365	8.9206 ± 0.4139	9.3785 ± 0.4628	0.080	-
	Cortical Thickness (mm)	0.7001 ± 0.0191	0.6811 ± 0.0306	0.6756 ± 0.0239	0.6683 ± 0.0239	0.764	-
	Polar Momment of Inertia (mm^4)	18.7315 ± 0.7439	20.2682 ± 1.4546	19.6494 ± 0.8299	20.3704 ± 0.8854	0.738	-
	BMD (mg HA/cm^3)	969.4624 ± 2.9323	972.7679 ± 7.7914	976.3143 ± 7.4967	963.6538 ± 2.6947	0.347	-

This table presents results of the vertebral microCT analyses. The upper rows present data obtained from cylindrical regions of trabecular bone in the vertebral bodies. The lower rows present data obtained from regions of cortical bone at the mid-point of the vertebral bodies. The first column lists the MicroCT parameters and the units. The next four columns present the group means ± standard error of the mean. The next column presents the p-values arising from between group comparisons performed using Kruskal-Wallis tests. The final column reveals the pairs that were found to be significantly different (a = Intact 0 vs. OVX 0; b = Intact 15 vs. OVX 0; c = Intact 15 vs. OVX 15; d = Intact 0 vs. OVX 15; e = OVX 0 vs. OVX 15). In addition, means that differ significantly have been presented in bold.